Article
Chinese Science Bulletin
Optics
September 2011 Vol.56 No.25: 2668–2673
doi: 10.1007/s11434-011-4642-5

Preparation and luminescence properties of $Y_2O_3:Er^{3+}/TiO_2$ with high specific surface area

YE YanXi[1*], LIU EnZhou[2*], HU XiaoYun[1†], YAN ZhiYun[1], JIANG ZhenYi[3] & FAN Jun[2]

[1] *Department of Physics, Northwest University, Xi'an 710069, China;*
[2] *School of Chemical Engineering, Northwest University, Xi'an 710069, China;*
[3] *Institute of Modern Physics, Northwest University, Xi'an 710069, China*

Received January 27, 2011; accepted April 8, 2011

The three composites $Y_2O_3:Er^{3+}$, $Y_2O_3:Er^{3+}/Yb^{3+}$ and $Y_2O_3:Er^{3+}/TiO_2$ were prepared using coprecipitation and sol-gel techniques. Their morphology, specific surface area, porosity, UV-vis. absorption spectra and fluorescence spectra were measured using SEM, TEM, surface analysis, UV-vis. absorption and photoluminescence spectrophotometry. SEM and TEM showed that samples prepared using coprecipitation were dispersed, while $Y_2O_3:Er^{3+}/TiO_2$ particles possessed a mesoporous surface and average diameter of about 10 nm. The specific surface area and porosity of $Y_2O_3:Er^{3+}/TiO_2$ did not result from the combination of the individual properties of $Y_2O_3:Er^{3+}$ and TiO_2. The specific surface area of $Y_2O_3:Er^{3+}/TiO_2$ was 135.991 m^2/g and was 4.8 times that of $Y_2O_3:Er^{3+}$ and 2.5 times that of Degussa P25 TiO_2. A high specific surface area is conducive for application to TiO_2 photocatalysis. The fluorescence spectra of the three composites exhibited three upconversion emission peaks with maxima at 237, 395 and 467 nm following excitation at 388, 500 and 570 nm, respectively.

Y_2O_3: Er^{3+}, TiO_2, specific surface area, upconversion luminescence, nanoporous materials

Citation: Ye Y X, Liu E Z, Hu X Y, et al. Preparation and luminescence properties of $Y_2O_3:Er^{3+}/TiO_2$ with high specific surface area. Chinese Sci Bull, 2011, 56: 2668–2673, doi: 10.1007/s11434-011-4642-5

Y_2O_3 is a good host material for luminescent agents because of its high chemical and photochemical stability, high melting point, potential for rare-earth doping and low phonon energy (430–500 cm^{-1}) [1,2]. Er^{3+} strongly absorbs throughout the infrared (IR)-ultraviolet (UV) range and thus is suitable for upconversion studies. Upconversion luminescence in Er^{3+}-doped host materials has been extensively studied due to their potential application in optical recording, solid-state lasers, solar cells, and biolabeling [3–7]. In the current study, $Y_2O_3:Er^{3+}$ was selected because of its favorable physicochemical and luminescence properties.

TiO_2 is often considered the most appropriate candidate for photocatalytic processes because of its relatively high photocatalytic reactivity, physical and chemical stability, low toxicity and cost effectiveness [8,9]. TiO_2 applications include sewage treatment, air purification and the photocatalytic reduction of CO_2. However the photocatalytic activity of TiO_2 is limited by its large band gap (3.0 and 3.2 eV for rutile and anatase phases, respectively). This causes TiO_2 to poorly absorb visible wavelength photons, and UV light (λ<387 nm, about 5% of the visible spectrum) is required to achieve photocatalysis by TiO_2. To extend the wavelength of light that TiO_2 absorbs, $Y_2O_3:Er^{3+}$ and $Y_2O_3:Er^{3+}/Yb^{3+}$ composites which can convert incident visible and IR wavelengths into UV wavelengths were prepared by coprecipitation. A $Y_2O_3:Er^{3+}/TiO_2$ composite was prepared using sol-gel techniques, to allow TiO_2 to absorb incident light. The UV-vis., specific surface area, porosity and upconversion properties of $Y_2O_3:Er^{3+}/TiO_2$, $Y_2O_3:Er^{3+}$ and Degussa P25 TiO_2 were studied and compared.

1 Materials and methods

1.1 Synthesis of $Y_2O_3:Er^{3+}$ and $Y_2O_3:Er^{3+}/Yb^{3+}$

Yttrium oxide, erbium oxide and ytterbium nitrate came

*These authors contributed equally to this work.
†Corresponding author (email: hxy3275@nwu.edu.cn)

from Rico rare earth metallurgy and functional materials national engineering research center Co., Ltd. (Baotou, China), butyl titanate was purchased from Kermel chemical reagents development canter (Tianjin, China), n-butanol was from BASF chemical Co., Ltd. (Tianjin, China), and acetic acid was from Hongyan chemical reagent factory (Tianjin, China). All chemicals were analytical grade and used without further purification.

Y_2O_3:Er^{3+} and Y_2O_3:Er^{3+}/Yb^{3+} were prepared by co-precipitation. Appropriate amounts of yttrium and erbium oxide were dissolved in 10 mL of nitric acid (65%) and the solution was stirred at reflux. When the solution was clear and transparent, the appropriate amount of ytterbium nitrate was added (solution A). Eighteen milliliters of ammonia (28%) was added dropwise and the solution was then stirred for 5 h. The solution was aged for 12 h and then centrifuged three times with distilled water and once with 25 mL ethanol absolute. The sample was heated at 140°C for 1 h to remove water, then 300°C for 1 h to remove ammonium nitrate, and finally annealed at in excess of 600°C for several hours to give Y_2O_3:Er^{3+}/Yb^{3+}. Y_2O_3:Er^{3+} was synthesized in a similar manner with the absence of ytterbium nitrate addition.

1.2 Preparation of Y_2O_3:Er^{3+}/TiO_2

Y_2O_3:Er^{3+}/TiO_2 was prepared by the sol-gel method. Solution B was prepared by mixing 6.4 mL of butyl titanate and 7.4 mL of n-butanol at room temperature for 30 min, then adding 4.6 mL of acetic acid and stirring for a further 6 h. Solution C was prepared as described above without the addition of ytterbium nitrate. Solution C was added dropwise to solution B, and the resulting solution was stirred for 2 h, aged for 48 h, centrifuged and dried. Y_2O_3:Er^{3+}/TiO_2 was obtained following annealing as described in Section 1.1.

1.3 Photocatalysis testing

TiO_2 or Y_2O_3:Er^{3+}/TiO_2 were dissolved in deionized water to give a turbid solution that was placed in a custom built reactor. Turbidity was maintained by passing gaseous carbon dioxide through the reactor. A Xe lamp at 1 m from the reactor was used as a light source. Carbinol was formed in the reaction solution during 8 h of photocatalysis and carbinol content was measured.

1.4 Characterization

Sample morphology was observed by thermal environment scanning electron microscopy (SEM, Quanta 400 FEG, FEI, Brno, Czech Republic) and transmission electron microscopy (TEM, TF20, FEI, Hong Kong). The specific surface area and porosity were measured with an automated surface area analyzer (NOVA 200e, Quantachrome Instruments, Miami, USA). UV-vis. absorption spectra were obtained on a UV-vis. spectrophotometer (UV-3600, Shimadzu, Tokyo, Japan). Upconversion luminescence was analyzed using a fluorescence spectrophotometer (F-7000, Hitachi, Tokyo, Japan, Xe lamp 150 W). Carbinol yield was analyzed by gas chromatography (GC-14C, Shimadzu, Soochow, Japan, with a hydrogen flame, PEG 20M column).

2 Results and discussion

2.1 EDS, EDAX, SEM and TEM imaging

Figure 1 shows the energy dispersive spectroscopy (EDS) patterns of Y_2O_3:Er^{3+} (Figure 1(a) with Er^{3+} molar ratio of 7.5%) and Y_2O_3:Er^{3+}/Yb^{3+} (Figure 1(b) with Er^{3+}/Yb^{3+} molar ratio of 5%/15%), and chemical formula were calculated according to the elemental contents shown in the inset tables. The formula of Y_2O_3:Er^{3+} was $Y_{0.79}Er_{0.07}O_{1.09}$ giving an Er^{3+}molar ratio of 8.1%, which was close to the intended content of 7.5%. The chemical formula of Y_2O_3:Er^{3+}/Yb^{3+} was $Y_{0.59}Er_{0.05}Yb_{0.09}O_{1.5}$ giving Er^{3+} and Yb^{3+} molar ratios of 6.8% and 12.3%, respectively, which were also close to the intended contents of 5% and 15%, respectively. This suggested that Er^{3+} and Yb^{3+} distributions within particles

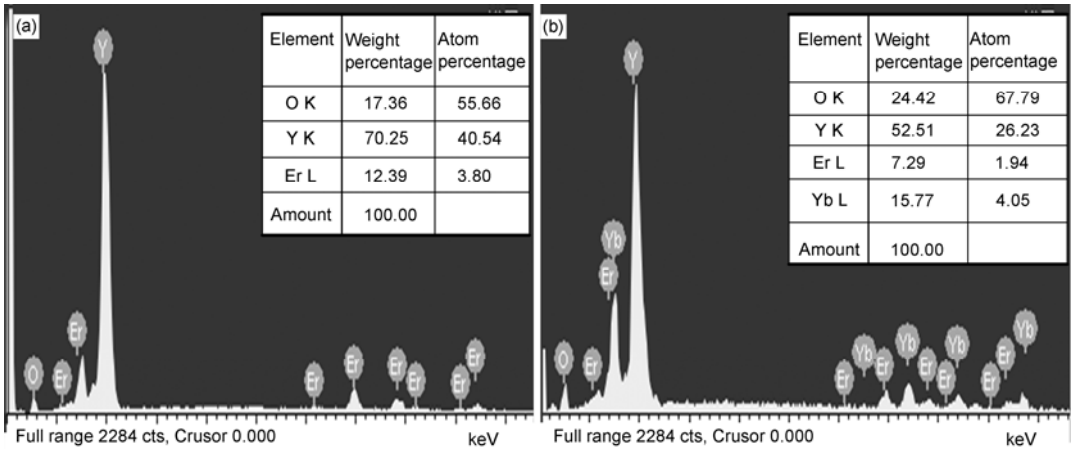

Figure 1 EDS spectra of Y_2O_3:Er^{3+} with Er^{3+} molar ratio of 7.5% (a) and Y_2O_3:Er^{3+}/Yb^{3+} with Er^{3+}/Yb^{3+} molar ratio of 5%/15% (b).

were uniform, which is favorable for preventing fluorescence quenching by Er^{3+} or Yb^{3+} agglomeration.

SEM images of Y_2O_3:Er^{3+} and Y_2O_3:Er^{3+}/Yb^{3+} are presented in Figure 2. The composites contained numerous small spheres with highly porous surfaces. To locate Er^{3+} and Yb^{3+} in the matrix, Y_2O_3:Er^{3+}/Yb^{3+}/TiO_2 was analyzed using TEM and scanning transmission electron microscopy (STEM) and the results are shown in Figure 3. The diameter of each particle was about 10 nm (Figure 3(a)). Nanoparticles were not well resolved in the SEM images because of agglomeration from annealing. Figure 3(b) shows that the surface of Y_2O_3:Er^{3+}/Yb^{3+}/TiO_2 appeared to be porous. Particles containing Er^{3+} and Yb^{3+} were not shown in Figure 3(b) and (c). The energy dispersive X-ray analysis (EDAX) image of the surface in Figure 3(d) indicated the presence of Er^{3+} and Yb^{3+}. This suggested that Er^{3+} and Yb^{3+} were distributed in pores and in the internal particle lattice, which prevented fluorescence quenching from surface defects and enhanced the luminescence efficiency.

2.2 Specific surface area and porosity

The surface pore size distributions of the samples are shown in Figure 4, where the curve with circles represents the

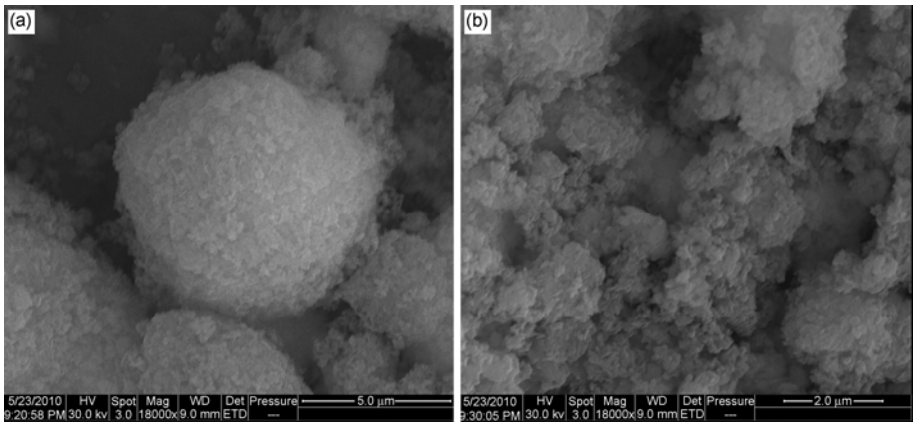

Figure 2 SEM images of Y_2O_3:Er^{3+} with Er^{3+} molar ratio of 7.5% (a) and Y_2O_3:Er^{3+}/Yb^{3+} with Er^{3+}/Yb^{3+} molar ratio of 5%/15% (b).

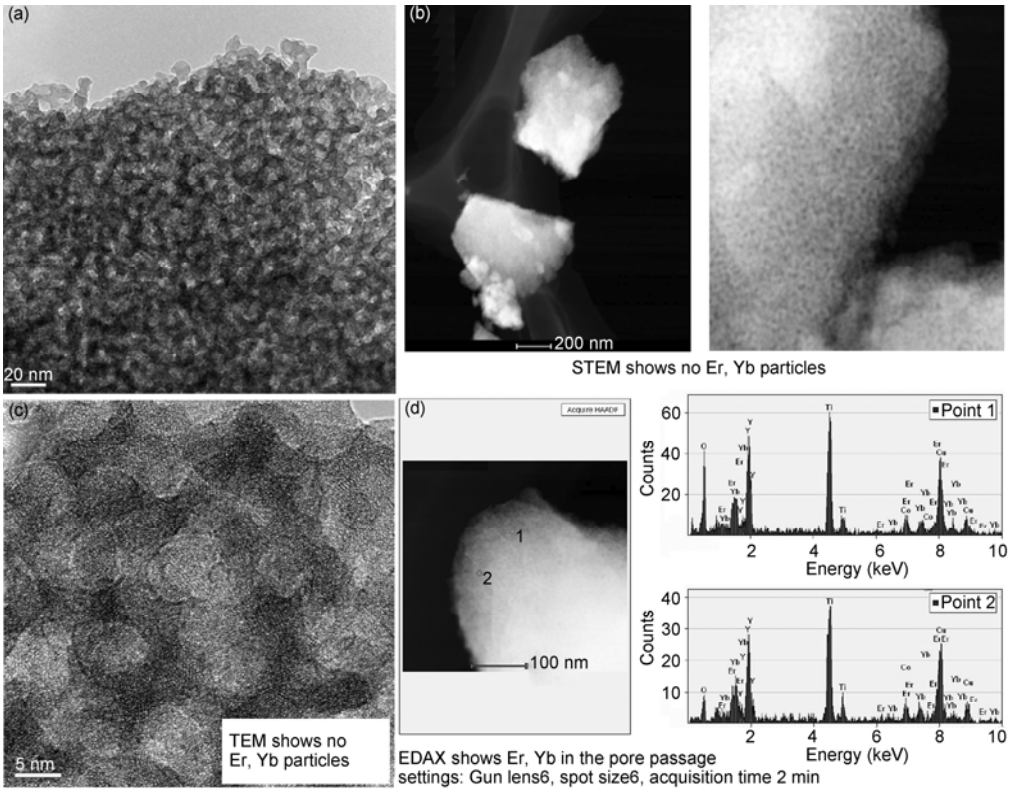

Figure 3 TEM images of Y_2O_3:Er^{3+}/Yb^{3+}/TiO_2. (a) High power TEM image; (b) high resolution TEM image; (c) high power STEM image; (d) EDAX image and spectra.

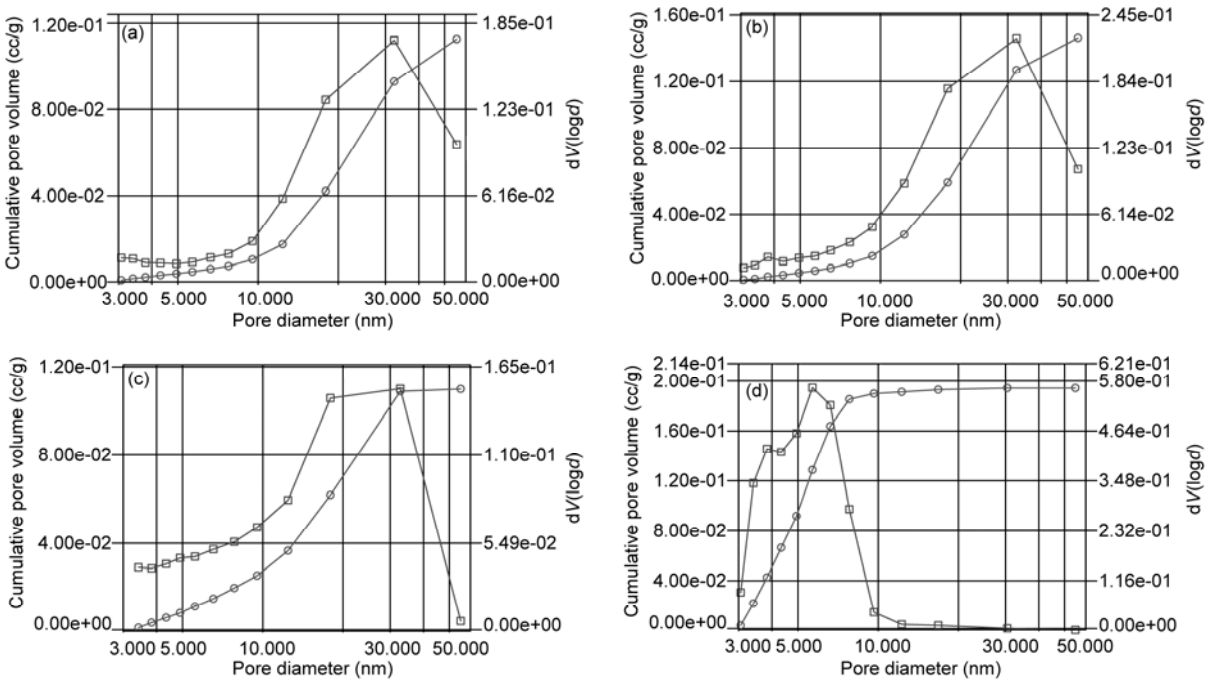

Figure 4 Porosity of Y_2O_3:Er^3 (a), Y_2O_3:Er^{3+}/Yb^{3+} (b), Degussa P25 TiO_2 (c) and Y_2O_3:Er^{3+}/TiO_2 (d).

accumulative pore volume, and the curve with squares represents the pore size distribution. The Kelvin equation was used to calculate the pore size:

$$r_k = \frac{-2\,\gamma\,V_m}{R\,T\,\ln(P/P_0)}, \quad (1)$$

where γ is the surface tension of nitrogen at 77 K (8.85 ergs/cm^2), V_m is the molar volume of liquid nitrogen (34.7 cm^3/mol), R is the molar gas constant (8.314 kJ/(kmol K), T is the boiling point of nitrogen (77 K), P/P_0 is the relative pressure of nitrogen, and r_k is the Kelvin pore radius. The specific surface areas and porosities are summarized in Table 1. The pore volume of Y_2O_3:Er^{3+}/TiO_2 was larger than those of Y_2O_3:Er^{3+} and Degussa P25 TiO_2, consistent with the STEM analysis. The specific surface area of Y_2O_3:Er^{3+}/TiO_2 was 135.991 m^2/g, which was 4.8 times higher than that of Y_2O_3:Er^{3+} and 2.5 times higher than that of Degussa P25 TiO_2. Thus, the properties of Y_2O_3:Er^{3+}/TiO_2 were not the simple combination of those of Y_2O_3:Er^{3+} and Degussa P25 TiO_2. The maximum N_2 adsorption capacity, pore volume and average pore diameter of Y_2O_3:Er^{3+}/TiO_2 were consistent with a highly porous material.

2.3 Fluorescence properties

Optical absorption spectra of Y_2O_3:Er^{3+}, Y_2O_3:Er^{3+}/TiO_2, Degussa P25 TiO_2 and Y_2O_3 obtained by diffuse reflection are shown in Figure 5. Five absorption peaks characteristic of Er^{3+} were observed in the spectrum of Y_2O_3:Er^{3+}, and were assigned to the $^4I_{15/2}\rightarrow{}^4G_{9/2}$ (365 nm), $^4I_{15/2}\rightarrow{}^4G_{11/2}$ (378 nm), $^4I_{15/2}\rightarrow{}^4F_{7/2}$ (489 nm), $^4I_{15/2}\rightarrow{}^2H_{11/2}$ (521 nm) and $^4I_{9/2}\rightarrow{}^2K_{15/2}$ (652 nm) transitions of Er^{3+}. Comparison of the optical absorption spectra of Y_2O_3:Er^{3+} and Y_2O_3 confirmed that these peaks arose from Er^{3+}, because they were absent in the spectrum of Y_2O_3. A peak at less than 400 nm in the spectrum of Y_2O_3:Er^{3+}/TiO_2 was due to the band gap of TiO_2. Only three absorption peaks characteristic of Er^{3+} appeared in the spectrum of Y_2O_3:Er^{3+}/TiO_2 (at 489, 521 and 652 nm). Absorptions at 365 and 377 nm were obscured by the optical transition of TiO_2. Absorptions from Er^{3+} appeared at higher energy in the spectrum of Y_2O_3:Er^{3+}/TiO_2 than in that for Y_2O_3:Er^{3+}, which reflected the high specific surface area of the composite containing TiO_2. This property is expected to increase its photocatalytic activity.

Y_2O_3:Er^{3+} was excited at each of the five absorptions

Table 1 Specific surface area and pore size distributions

Sample	Y_2O_3:Er^{3+}	Y_2O_3:Er^{3+}/Yb^{3+}	Degussa P25 TiO_2	Y_2O_3:Er^{3+}/TiO_2 composite
Specific surface area (m^2/g)	28.380	33.423	53.641	135.991
Average pore diameter (nm)	17.909	17.885	3.420	3.832
Maximum adsorption capacity of N_2 (mL/g)	1.40×10^{-1}	1.00×10^{-1}	1.00×10^{-1}	1.90×10^{-1}
Pore volume (mL/g)	0.113	0.146	0.110	0.194
Most common pore diameter (nm)	32	32	32	7

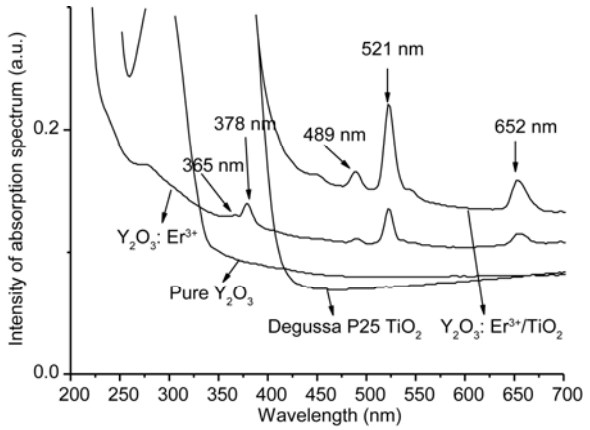

Figure 5 Diffuse reflectance UV-vis absorption spectra.

(365, 378, 489, 521 and 652 nm). Down-conversion luminescence was observed upon excitation at 365, 377 and 521 nm, while upconversion luminescence occurred upon excitation at 388 nm (in the middle of the absorption peak at 377 nm) and 500 nm (in the middle of the absorption peak at 521 nm). The photon energy may have been converted to lattice vibrations and heat radiation upon excitation at 489 and 652 nm.

Upconversion luminescence spectra of Y_2O_3:Er^{3+} containing 2% Er^{3+} after calcination obtained on excitation at 388, 500 and 570 nm are shown in Figure 6. The efficiency of upconversion luminescence is typically extremely low, so absorptions at 388, 500 and 570 nm were not strongly apparent in the UV-vis spectra in Figure 5. Emission peaks at 237, 395 and 467 nm arose from the transitions $^4D_{3/2}\rightarrow{}^4I_{15/2}$, ($^2G$, ^4F, ^2H) $_{9/2}\rightarrow{}^4I_{15/2}$ and $^4F_{5/2}\rightarrow{}^4I_{15/2}$, respectively (Figure 7).

The upconversion luminescence intensities of Y_2O_3:Er^{3+}, Y_2O_3:Er^{3+}/Yb^{3+} and Y_2O_3:Er^{3+}/TiO_2 upon excitation at 388, 500 and 570 nm are shown in Figure 8. Comparison of these spectra shows that the photosensitization of Yb^{3+} under excitation by UV and blue light was inferior to that under IR light [3,10,11]. Y_2O_3:Er^{3+}/TiO_2 still exhibited three

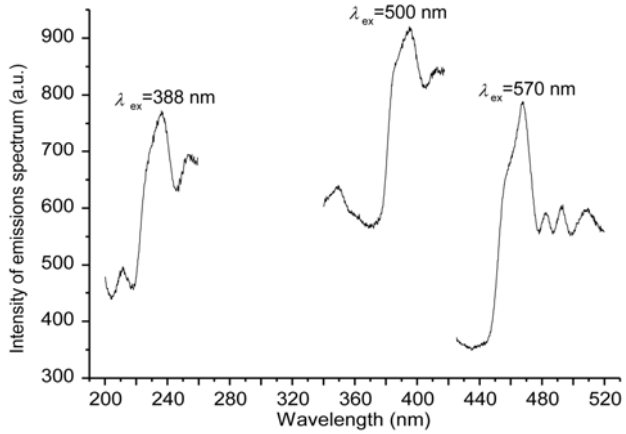

Figure 6 Upconversion luminescence spectra of Y_2O_3:Er^{3+} containing 2% Er^{3+} upon excitation at 388, 500 and 570 nm.

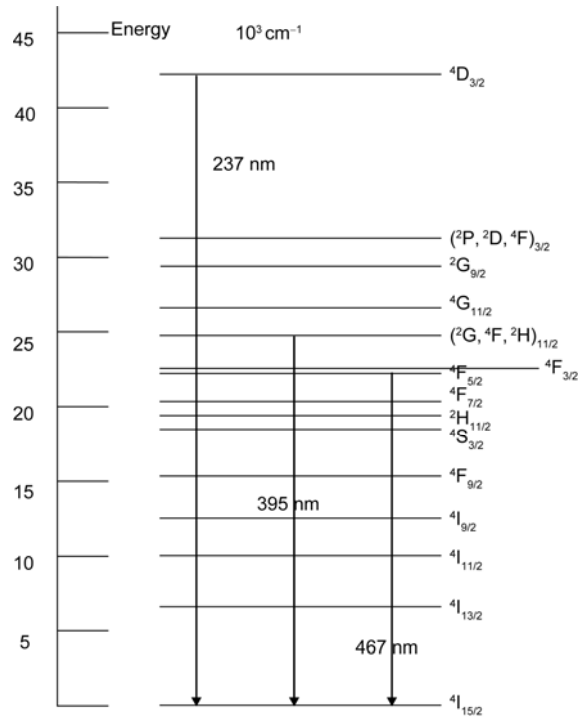

Figure 7 Energy level diagram for Er^{3+}.

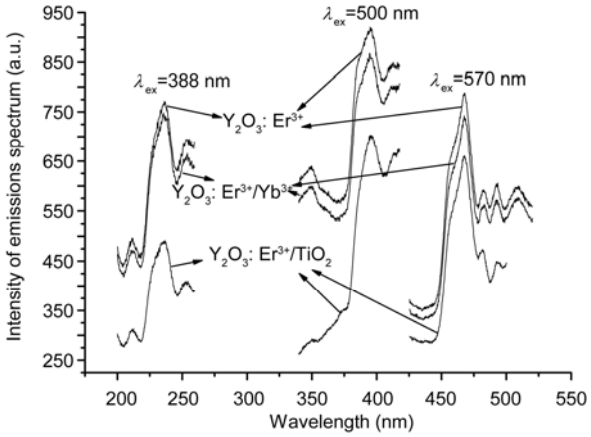

Figure 8 Upconversion luminescence spectra of Y_2O_3:Er^{3+}, Y_2O_3:Er^{3+}/Yb^{3+} and Y_2O_3:Er^{3+}/TiO_2 upon excitation at 388, 500 and 570 nm.

emission peaks, but their relative emission intensities were lower than those of Y_2O_3:Er^{3+} and Y_2O_3:Er^{3+}/Yb^{3+}. Y_2O_3:Er^{3+}/ TiO_2 could convert low energy photons to those of higher energy, which is beneficial for nanosized TiO_2 photocatalysis.

2.4 Methanol formation by photocatalysis

Eq. (2) outlines the formation of methanol by fixation of CO_2 using TiO_2 and Y_2O_3:Er^{3+}/TiO_2 as photocatalysts.

$$CO_2+H_2O\xrightarrow[Y_2O_3:\,Er^{3+}/TiO_2\ \text{composite}]{TiO_2\ \text{or}}CH_3OH \qquad (2)$$

During the course of the experiments, some reaction solu-

tion evaporated to give a condensed solution. The contents of methanol in the reaction and condensed solutions after photocatalysis by TiO_2 or Y_2O_3:Er^{3+}/TiO_2 are shown in Table 2. Y_2O_3:Er^{3+}/TiO_2 was clearly a more effective photocatalyst for this reaction than TiO_2.

Table 2 Methanol content after fixation of CO_2 by photocatalysis using TiO_2 and Y_2O_3:Er^{3+}/TiO_2

	Pure TiO_2	Y_2O_3:Er^{3+}/TiO_2 composite
Reaction solution (μmol/g)	47.6	79.7
Condensed solution (μmol/g)	50.0	110.7

3 Conclusions

Disperse Y_2O_3:Er^{3+} and Y_2O_3:Er^{3+}/Yb^{3+} were prepared by coprecipitation, and Y_2O_3:Er^{3+}/TiO_2 was prepared by the sol-gel method. Y_2O_3:Er^{3+}/TiO_2 particles contained numer ous mesopores on their surfaces, had an average diameter of about 10 nm, and a specific surface area of 135.991 m^2/g, which was 4.8 times that of Y_2O_3: Er^{3+} and 2.5 times that of Degussa P25 TiO_2. Five UV-vis absorptions were observed for Y_2O_3:Er^{3+}, and fluorescence spectra revealed that this composite exhibited three upconversion emission peaks, with maximum emission wavelengths at 237, 395 and 467 nm upon excitation at 388, 500, and 570 nm, respectively. The Y_2O_3:Er^{3+}/TiO_2 composite showed higher photocatalytic activity than TiO_2.

This work was supported by the National Natural Science Foundation of China (20876125), the Research Fund for the Doctoral Program of Higher Education of China (20096101110013), the Natural Science Foundation of Shanxi Province (2010JZ002), and the Northwest University Graduate Cross-discipline Fund (09YJC27 and 09YJC24).

1 Zhang J, Wang S W, An L Q, et al. Up-conversion luminescence in Yb^{3+}, Er^{3+}:Y_2O_3 nanocraystalline powders excited by a 980 nm laser diode (in Chinese). Chin J Lumin, 2005, 26: 789–793
2 Pang T, Cao W H, Xing M M, et al. Preparation and luminescence properties of monodisperse silica/aminosilane-coated Y_2O_3:Yb,Ho upconversion nanoparticles. Chinese Sci Bull, 2011, 56: 137–141
3 Yanes A C, Santana-Alonso A, Mendez-Ramos J, et al. Yb^{3+}-Er^{3+} co-doped sol-gel transparent nano-glass-ceramics containing $NaYF_4$ nanocrystals for tuneable up-conversion phosphors. J Alloy Compd, 2009, 480: 706–710
4 Rapaport A, Milliez J, Bass M, et al. Review of the properties of up-conversion phosphors for new emissive displays. J Display Tech, 2006, 2: 68–78
5 Pang T, Cao W H. Up-conversion luminescence of Er^{3+} doped and Er^{3+}/Yb^{3+} co-doped $YTaO_4$. Chinese Sci Bull, 2008, 53: 178–182
6 Tikhomirov V K, Mortier M, Gredin P, et al. Preparation and up-conversion luminescence of 8 nm rare-earth doped fluoride nanoparticles. Opt Express, 2008, 16: 14544–14549
7 Xie G X, Lin J M, Wu J H, et al. Application of upconversion luminescence in dye-sensitized solar cells. Chinese Sci Bull, 2011, 56: 96–101
8 Xu F X, Feng G J, Liu S W, et al. A study of visible light photocatalytic activity of nano TiO_2 doped with up-conversion luminescence agent (in Chinese). Bull Chin Ceram Soc, 2008, 27: 1140–1145
9 Wang J, Ma T, Zhang G, et al. Preparation of novel nanometer TiO_2 catalyst doped with up-conversion luminescence agent and investigation on degradation of acid red B dye using visible light. Catal Commun, 2007, 8: 607–611
10 Qiu J B, Song Z G. Nanocrystals precipitation and up-conversion luminescence in Yb^{3+}-Tm^{3+} co-doped oxyfluoride glasses. J Rare Earth, 2008, 26: 919–923
11 Liang L F. Up-conversion properties and morphology analysis of Yb^{3+}/Er^{3+} (or Tm^{3+}) codoped fluorides (in chinese). Doctoral Dissertation. Guangzhou: Sun Yat-sen University, 2005. 1–164